IEEE Access
Multidisciplinary ⋮ Rapid Review ⋮ Open Access Journal

Received December 19, 2020, accepted January 14, 2021, date of publication January 26, 2021, date of current version February 1, 2021.

Digital Object Identifier 10.1109/ACCESS.2021.3054647

Phase Shaping Method for Negative Input Admittance of Buck Converter Based on Sliding Mode Disturbance Observer

XUZHOU ZHUANG, (Graduate Student Member, IEEE), QINJIN ZHANG, (Member, IEEE), YANCHENG LIU, PENGLI ZHU, (Graduate Student Member, IEEE), XIANGLU ZHENG, YUJI ZENG, HAOHAO GUO, AND ZHENRUI ZHANG, (Graduate Student Member, IEEE)
Marine Engineering College, Dalian Maritime University, Dalian 116026, China

Corresponding author: Qinjin Zhang (zqj20@dlmu.edu.cn)

This work was supported in part by the National Natural Science Foundation (NNSF) of China under Grant 51979021 and Grant 51709028, in part by the Fundamental Research Funds for the Central Universities under Grant 3132019317, and in part by the double first-class construction Funds under Grant BSCXXM009.

ABSTRACT The power electronic converter that supplies power to the unmanned ship's servers can cause self-excited oscillation of the LC input filter under heavy load. To suppress voltage oscillation, an input impedance shaping method based on a sliding mode disturbance observer is presented. The self-excited oscillation mechanism of the LC filter caused by the buck converter's positive feedback is analyzed by using the small-signal model. The sliding mode disturbance observer calculates the input voltage according to the output voltage, inductance current and duty cycle of the buck converter. The feedforward compensation of the observed voltage reshapes the input admittance of the buck converter, making the system not meet the conditions of self-excited oscillation and suppressing the voltage oscillation of the LC filter. The phase shaping of input admittance is compared with the traditional amplitude shaping by the Bode diagram and Nyquist diagram. The experimental results show that the phase shaping method could better suppress the LC filter's self-excited oscillation and the sliding mode disturbance observer reduced the hardware cost.

INDEX TERMS Sliding mode disturbance observer, impedance shaping, constant power load, self-excited oscillation, positive feedback.

I. INTRODUCTION

Power electronic converter will play an essential role in the fields of microgrid, data center, aircraft and ship with the development of semiconductor technology [1]–[3]. Due to the advantages of simple control, high efficiency, strong robustness and high reliability, DC power supply is more suitable for the servers of unmanned ships in complex and changeable ocean weather. In order to suppress harmonic current, power electronic load should be connected to the DC bus through an input filter. However, the cascading of input filter and power electronic converter may cause system resonance, resulting in a voltage oscillation and affecting the safety of electrical equipment [4]–[6].

The instantaneous input power of the converter is constant under the action of closed-loop control, so the power electronic converter is called constant power load (CPL) [7], [8]. However, CPL exhibits negative impedance characteristics, which reduces the damping and degrades the stability margin [9], [10]. Several solutions have been proposed to mitigate the issue. When a single power converter directly supplies power to an independent CPL, the current harmonics of the load converter are suppressed by the filter inside the source converter, so no LC low-pass filter is needed between the two converters. For the instability of this cascade system, the damping factor estimation algorithm [11] and the negative impedance detection method [12] can be used to compensate for the system damping adaptively in real-time. Moreover, the fast state-plane-based source-end controller solves bus voltage oscillation caused by constant power load and improves the dynamic performance [13]. Since the constant power load is a non-linear load, various non-linear control methods have been proposed. The adaptive backstepping control strategy based on extended Kalman filter

The associate editor coordinating the review of this manuscript and approving it for publication was Fanbiao Li.

can be used to observe the disturbance and compensate the output voltage [14]. When the noise has unknown statistical characteristics or the system is uncertain, the result of Kalman filter is not ideal, but H∞ filter not only has high estimation accuracy but also has robustness [15], [16]. Furthermore, to further improve the dynamic performance and robustness, an adaptive back-stepping sliding mode control strategy based on precise feedback linearization is proposed [17]. In summary, the instability of such systems is mainly caused by the interaction between the constant power load and the LC filter in the upstream converter. The stability control method for this situation has achieved excellent results.

The application of multiple source converters and multiple load converters is more common. In this kind system, the current harmonics can affect the current sharing stability of the source converter and the reliable operation of other load converters since the input current of the load converter is a trapezoidal wave. The load converter should be connected to the DC bus through the LC input filter. However, constant power load is more likely to cause self-excited oscillation of the LC input filter. A virtual negative impedance control strategy based on the non-linear disturbance observer is proposed to counteract line inductance and enhance system damping [18]–[20]. Nevertheless, the virtual negative inductance needs to be greater than the equivalent line inductance when the resonant frequency of the LC filter is larger than the control bandwidth of the source converter, which would reduce the load disturbance suppression effect of the source converter. Meanwhile, the large-signal stability of the system after adding virtual impedance is studied by the Brayton–Moser mixed potential analysis [21]. Unfortunately, this method reduces the disturbance suppression ability in the specific frequency band. Aiming at the defects of the classical control theory, a model predictive control based on Takagi Sugeno fuzzy model is proposed in [22]. The extended Kalman algorithm is used to estimate the load power in real time, and then the model predictive control is used to coordinate the power converter and the load converter. However, this method is more suitable for small-scale systems with a stable structure. When the constant power load is an inverter, the virtual impedance is established in the inverter through voltage feedforward. The virtual impedance is effective near the resonant frequency of the LC input filter, which improves the damping of the system [5], [23]. The compensation signal is directly added to the inverter's PWM link without passing through the current loop [24]. This method has little influence on the control closed-loop to make a better trade-off between the DC bus's voltage stability and the dynamic performance of load. Due to the compensation signal bypassing the current loop, the current limiting function is lost, and the converter is easy to enter the overshoot or even trip. The voltage feedforward can be used to establish the virtual impedance in converter when the constant power load is DC/DC converter, which can also improve system damping [25]. At present, feedforward compensation only changes the amplitude characteristics of the negative incremental impedance of constant power load in a specific frequency range. However, it is difficult to shape the impedance amplitude in many cases. In addition, the feedforward methods for stabilization of inverter or DC/DC converter require additional sensors to measure the input voltage, which undoubtedly increases the hardware cost.

This paper focuses on the stability analysis and improvement of the dc cascaded system. The studied dc cascaded system is composed of a buck converter and an LC input filter in the unmanned ship. Mechanism analysis shows that the positive feedback between buck converter and LC input filter is the main cause of self-excited oscillation. The input voltage disturbance is observed and then the damping current is injected into the current inner loop through the filter, and then the phase of the input admittance is changed by adjusting the inductance current. The sliding mode observer reduces the hardware cost by replacing the input voltage sensor and the phase shaping method suppresses the self-excited oscillation of the LC filter. The rest of this paper is organized as follows: In Section II, the positive feedback effect and self-excited oscillation mechanism between the buck converter and LC input filter are analyzed. Moreover, the sliding mode disturbance observer is proposed to observe the input voltage of buck converter, and the stability and convergence of the observer are analyzed in Section III. The input admittance shaping method of input admittance is proposed and compared with the amplitude shaping method in Section IV. Then the experiment results are presented to verify the effectiveness of the proposed control strategy in Section V. Finally, the achievements are summarized in section VI.

II. SELF-EXCITED OSCILLATION OF THE LC FILTER UNDER CONSTANT POWER LOAD

Communication devices and servers are the core equipments of unmanned ships, and their power supply stability is crucial. Due to the reliability and standardization of the 48V DC power supply, it is adopted by various communication devices and servers, but there are also a large number of 24V powered devices. Electronic load and PWM based DC-DC converter could produce high-frequency current harmonics due to high-frequency switching characteristics. In order to prevent the current harmonics between converters, the load converter needs an LC input filter connected to the DC bus. The power supply structure is shown in Fig.1(a).

Fig.1(b) shows the cascade structure of the LC input filter and buck converter. L_f and C_f are inductance and capacitance of the LC input filter respectively. R_f and R_{Cf} are inductance parasitic resistance and capacitance parasitic resistance of the LC input filter respectively. L, C and R are inductance, capacitance and load resistance of buck converter respectively. R_L and R_C are inductance parasitic resistance and capacitance parasitic resistance of buck converter respectively. i_{dc} and i_B are the input current of the LC input filter and buck converter respectively. v_{dc} is the DC-bus voltage and v_B is the input voltage of the buck converter. v_o is the output voltage of the

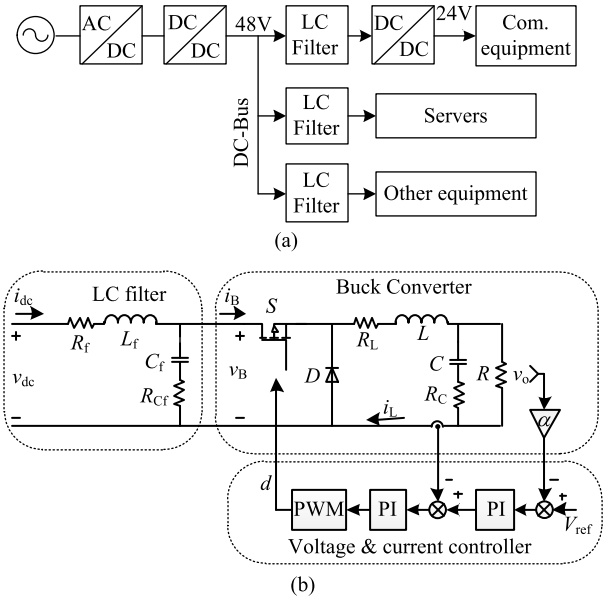

FIGURE 1. Power supply system for unmanned ship conducting equipment and server: (a) Power supply structure of communication equipment and server, (b) buck converter with an LC input filter.

buck converter and α is the feedback coefficient of the output voltage.

The complex frequency domain analysis in this paper uses the small signal analysis method to linearize the non-linear system. Assuming that the converter near the steady-state operating point can be approximated as a linear system when the disturbance is small, then a small-signal linear dynamic model of the converter is established in the complex frequency domain for stability analysis.

The transfer function of the LC input filter is

$$G_{\mathrm{f}}(s)=\frac{R_{\mathrm{Cf}}C_{\mathrm{f}}s+1}{L_{\mathrm{f}}C_{\mathrm{f}}s^{2}+\left(R_{\mathrm{f}}+R_{\mathrm{Cf}}\right)C_{\mathrm{f}}s+1} \tag{1}$$

The input current of the LC input filter is

$$i_{\mathrm{dc}}(s)=G_{\mathrm{f}}(s)\,i_{\mathrm{B}}(s) \tag{2}$$

The output voltage of the LC input filter is

$$v_{\mathrm{B}}(s)=G_{\mathrm{f}}(s)\,v_{\mathrm{dc}}(s) \tag{3}$$

The natural oscillation frequency of the LC input filter is

$$f_{\mathrm{r}}=1\Big/\left(2\pi\sqrt{L_{\mathrm{f}}C_{\mathrm{f}}}\right) \tag{4}$$

From formula (2) and (3), it can be seen that the LC input filter has a low-pass characteristic from the bus voltage v_{dc} to the voltage v_{B}, while the LC input filter has a low-pass characteristic from the current i_{B} to the bus current i_{dc}. Therefore, the low-pass filter can suppress bus voltage interference on the load, and also can suppress the interference of load current harmonics on other equipment. However, the buck converter with voltage closed-loop control shows negative incremental impedance at the balance point, which causes LC filter output voltage oscillation.

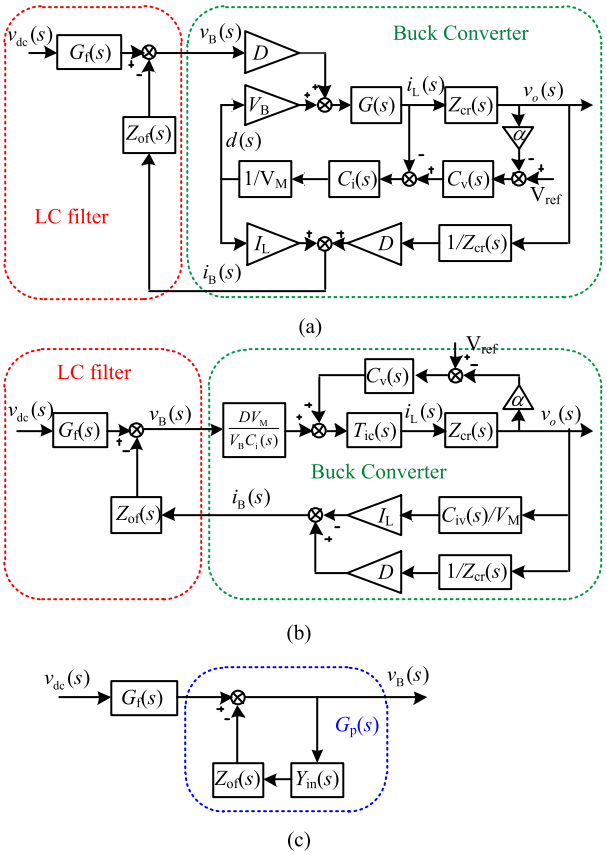

FIGURE 2. Control block diagram of a cascade system of LC filter and buck converter: (a) Control diagram of LC Input Filter and buck Converter, (b) Equivalent control block diagrams, (c) Impedance model.

Fig.2 shows the equivalent model of LC input filter and buck converter. The transfer function from duty cycle $d(s)$ to inductance current $i_{\mathrm{L}}(s)$ is

$$G(s)=\frac{\left(R+R_{C}\right)Cs+1}{\left(R+R_{C}\right)LCs^{2}+\left(L+RR_{L}C+R_{C}R_{L}C+RR_{C}C\right)s+R+R_{L}} \tag{5}$$

The transfer function from inductance current $i_{\mathrm{L}}(s)$ to output voltage $v_{\mathrm{o}}(s)$ to is

$$Z_{\mathrm{cr}}(s)=\frac{v_{\mathrm{o}}(s)}{i_{\mathrm{L}}(s)}=\frac{RR_{C}Cs+R}{\left(R+R_{C}\right)Cs+1} \tag{6}$$

The closed-loop transfer function of inductance current of the buck converter is

$$T_{\mathrm{ic}}(s)=\frac{V_{\mathrm{B}}G(s)C_{\mathrm{i}}(s)/V_{\mathrm{M}}}{1+V_{\mathrm{B}}G(s)C_{\mathrm{i}}(s)/V_{\mathrm{M}}} \tag{7}$$

where V_{B} is the DC steady-state component of the input voltage v_{B}, and $1/V_{\mathrm{M}}$ is the gain of the PWM link.

The closed-loop transfer function of voltage is

$$T_{\mathrm{vc}}(s)=\frac{C_{\mathrm{v}}(s)T_{\mathrm{ic}}(s)Z_{\mathrm{cr}}(s)}{1+\alpha C_{\mathrm{v}}(s)T_{\mathrm{ic}}(s)Z_{\mathrm{cr}}(s)} \tag{8}$$

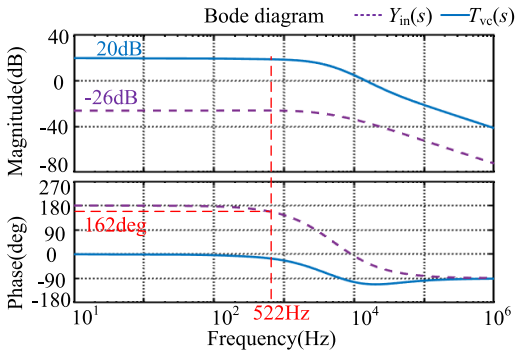

FIGURE 3. Bode diagram of $T_{vc}(s)$ and $Y_{in}(s)$.

As shown in Fig.2(b), the output voltage of the buck converter becomes

$$v_o(s) = \frac{DV_M T_{vc}(s)}{V_B C_i(s) C_v(s)} v_B(s) \tag{9}$$

where D is the steady-state component of the duty cycle.

The input current of the buck converter is

$$i_B(s) = \left(-\frac{I_L C_{iv}(s)}{V_M} + \frac{D}{Z_{cr}(s)} \right) v_o(s) \tag{10}$$

where $C_{iv}(s) = \alpha C_v(s) C_i(s) + C_i(s) Z_{cr}(s)$ is the series equivalent transfer function of the voltage and current controllers.

The input admittance of buck converter is obtained by combining equations (9) and (10)

$$Y_{in}(s) = \left(-\frac{I_L C_{iv}(s)}{V_M} + \frac{D}{Z_{cr}(s)} \right) \frac{DV_M T_{vc}(s)}{V_B C_i(s) C_v(s)} \tag{11}$$

The admittance of the closed-loop buck converter in formula (11) consists of two parts, one of which produces negative admittance

$$Y_{in}^{-}(s) = -\frac{I_L C_{iv}(s) D T_{vc}(s)}{V_B C_i(s) C_v(s)}$$

The other part produces positive admittance

$$Y_{in}^{+}(s) = \frac{V_M D^2 T_{vc}(s)}{V_B C_i(s) C_v(s) Z_{cr}(s)}$$

In order to quantitatively analyze the input admittance characteristics of the buck converter, the Bode diagram of the closed-loop transfer function and input admittance of the buck converter is drawn in Fig.3. The parameters are shown in Table 1. Within the closed-loop bandwidth of buck converter, the amplitude of the closed-loop transfer function is 20dB (the gain is 10) and the phase is zero. Therefore, the output voltage can be stabilized at 24V at a given value of 2.4V. The amplitude of the input admittance is −26dB, and the phase is 180deg. The input admittance is −0.05S within the closed-loop bandwidth.

The output impedance of the LC input filter is

$$Z_o(s) = \frac{R_{Cf} L_f C_f s^2 + (L_f + R_{Cf} R_f C_f) s + R_f}{L_f C_f s^2 + (R_f + R_{Cf}) C_f s + 1} \tag{12}$$

TABLE 1. Parameters of buck converter and LC filter.

Symbol	Description	Value
v_{dc}	Input voltage	48 V
v_o	output voltage	24 V
V_{ref}	reference voltage	2.4 V
α	Feedback coefficient	0.1
L	Inductance of buck Converter	50μH
C	Capacitance of buck Converter	360μF
R	Load resistance	5Ω
f_s	switching frequency	20 kHz
V_M	Sawtooth amplitude value	3 V
$C_i(s)$	Current controller	0.2+300/s
$C_v(s)$	Voltage controller	50+2000/s
L_f	Inductance of LC filter	770μH
C_f	Capacitance of LC filter	120μF
R_f	Resistance of LC filter	0.25Ω
f_r	Resonant frequency of LC filter	522 Hz

According to Kirchhoff's Voltage Law and Ohm's Law, it can be obtained in the frequency domain

$$\begin{cases} v_B(s) = v_{dc}(s) G_f(s) - i_B(s) Z_{of}(s) \\ i_B(s) = v_B(s) Y_{in}(s) \end{cases} \tag{13}$$

The transfer function from the input voltage $v_{dc}(s)$ to the output voltage $v_B(s)$ of the LC input filter is

$$\frac{v_B(s)}{v_{dc}(s)} = G_f(s) \frac{1}{1 + Z_{of}(s) Y_{in}(s)} \tag{14}$$

The impedance model as shown in Fig. 2 (c) is obtained by formula (14). The input admittance of the buck converter and the output impedance of the LC filter constitutes the feedback link

$$G_p(s) = \frac{1}{1 + Z_{of}(s) Y_{in}(s)} \tag{15}$$

The negative admittance of buck converter makes the link $G_p(s)$ become positive feedback, which is easy to cause self-excited oscillation of the system. Self-excited oscillation is a stable and continuous oscillation produced by itself without an external excitation signal. According to the principle of self-oscillator in analog electronic technology, the balance conditions for generating self-oscillation are

$$\begin{cases} |Z_{of}(s) Y_{in}(s)| = 1 \\ \angle Z_{of}(s) + \angle Y_{in}(s) = (2n+1)\pi, n = 0, \pm 1, \pm 2, \cdots \end{cases} \tag{16}$$

The starting conditions of self-excited oscillation are

$$\begin{cases} |Z_{of}(s) Y_{in}(s)| > 1 \\ \angle Z_{of}(s) + \angle Y_{in}(s) = (2n+1)\pi, n = 0, \pm 1, \pm 2, \cdots \end{cases}$$

Fig.4(a) shows the Bode diagram of the impedance ratio $Z_{of}(s)Y_{in}(s)$. The amplitude of the impedance ratio $Z_{of}(s)Y_{in}(s)$ is 2dB ($|Z_{of}(s)Y_{in}(s)| = 1.26$) and the phase is $\angle Z_{of}(s) + \angle Y_{in}(s) = \pi$ at the resonant frequency (522Hz) of the LC input filter. The Nyquist curve of the system surrounds the (−1,0) point and the system is unstable when starting conditions of self-excited oscillation are satisfied, as shown in Fig.4(b).

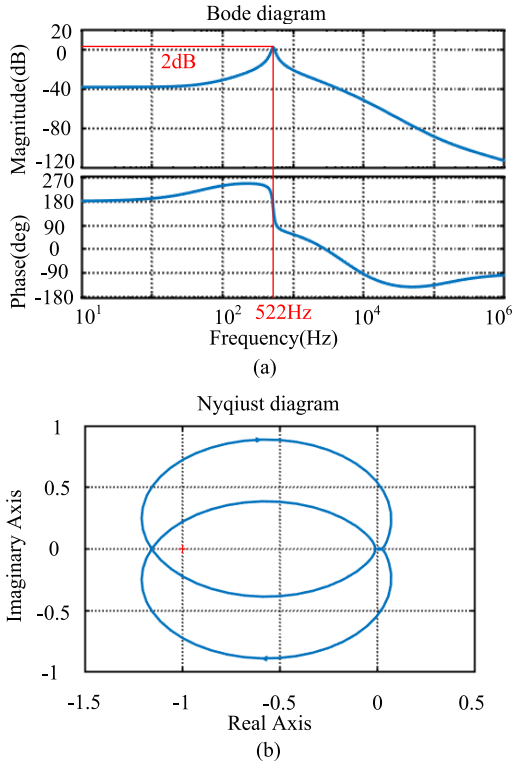

FIGURE 4. Bode diagram and Nyquist diagram of $Z_{of}(s)Y_{in}(s)$: (a) Bode diagram, (b) Nyquist diagram.

III. SLIDING MODE DISTURBANCE OBSERVER

Fig.5(a) is the structure diagram of the input admittance shaping method. This method adds the observed input voltage of the buck converter to the given value of the current inner loop through a filter, then changes the input admittance of the buck converter by adjusting the inductance current. This method could change the amplitude or phase of the admittance $Y_{in}(s)$ to make the system not meet the starting conditions of self-excited oscillation and then suppress the self-excited oscillation of the LC filter. This method reduces the hardware cost by reducing a sensor that detects the input voltage. Besides, the influence of the proposed method on the output voltage of the converter is quite limited due to this method compensates in the inner current loop.

When the inductance loss is ignored, the inductance current of the buck converter is

$$L\frac{di_L(t)}{dt} = v_B(t)d(t) - v_o(t) \tag{17}$$

Furthermore, the equation (17) is linearized and the quadratic term is ignored

$$L\frac{di_L(t)}{dt} = Dv_B(t) - DV_B + V_B d(t) - v_o(t) \tag{18}$$

The control variable is defined as

$$u(t) = V_B d(t) - v_o(t) \tag{19}$$

There are two kinds of disturbances in Buck Converter: input voltage and load current. The input voltage disturbance is

$$\phi = Dv_B(t) - DV_B \tag{20}$$

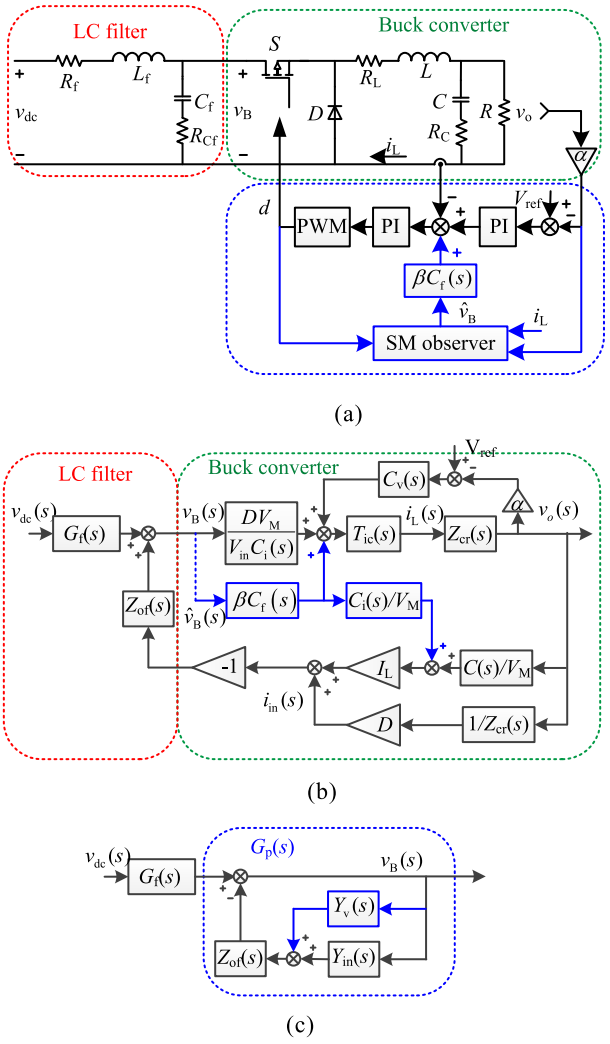

FIGURE 5. Feedforward Compensation and Equivalent Control Block Diagram of buck Converter: (a) Feedback compensation based on sliding mode disturbance observer, (b) Equivalent control block diagram for feedforward compensation, (c) Impedance model after feedforward compensation.

In order to estimate ϕ, a sliding mode observer is introduced

$$\frac{d\hat{i}_L(t)}{dt} = \frac{\sigma}{L}\mathrm{sgn}\left[i_L(t) - \hat{i}_L(t)\right] + \frac{1}{L}V_B d(t) - \frac{1}{L}v_o(t) \tag{21}$$

where $\hat{i}_L(t)$ is the observed inductance current, σ denotes the designed variable.

The sliding surface of the sliding mode observer is defined as

$$S(t) = i_L(t) - \hat{i}_L(t) \tag{22}$$

According to formulas (18), (21) and (22), it can be concluded that

$$\frac{dS(t)}{dt} = \frac{\phi}{L} - \frac{\sigma}{L}\mathrm{sgn}S(t) \tag{23}$$

The observed value of input voltage disturbance of buck converter is

$$\hat{\phi} = L\frac{dS(t)}{dt} + \sigma\mathrm{sgn}S(t) \tag{24}$$

The observed input voltage of the buck converter is

$$\hat{v}_{\mathrm{B}}(t) = V_{\mathrm{B}} + \frac{L}{D}\frac{dS(t)}{dt} + \frac{\sigma}{D}\mathrm{sgn}\, S(t) \tag{25}$$

To ensure the admittance shaping method's effectiveness, the stability of the sliding mode observer must be guaranteed first. Consider the following Lyapunov functions:

$$V = \frac{1}{2}S^2(t) \tag{26}$$

The derivative of the formula (26) is

$$\begin{aligned} \dot{V} &= S(t)\dot{S}(t) = \frac{1}{L}S(t)\left[\phi - \sigma sgn\, S(t)\right] \\ &\le \frac{1}{L}|S(t)|\left(|\phi| - \sigma\right) \end{aligned} \tag{27}$$

If σ satisfies the following conditions

$$|\phi| + \eta < \sigma, \eta > 0 \tag{28}$$

then

$$\dot{V} \le -\frac{\eta}{L}|S(t)| \tag{29}$$

Selecting a large enough σ can not only ensure that the observer is asymptotically stable but also increase the observer bandwidth. Although the increase of σ also causes high frequency chatting of the observer output, the filter of the feedforward channel can suppress the high-frequency clutter.

In order to ensure the dynamic response performance of the system, the sliding surface $S = 0$ should be reachable in finite time [26], [27]. Suppose that $S(0) \neq 0$ at the initial moment and $S(t_{\mathrm{r}}) = 0$ after time t_{r}. According to formula (29), when $S \ge 0$, $\dot{S} \le -\frac{\eta}{L}$, both sides are integrated at the same time

$$\begin{cases} \int_{S(0)}^{S(t_{\mathrm{r}})} dS \le \int_0^{t_{\mathrm{r}}} -\frac{\eta}{L}dt \\ S(t_{\mathrm{r}}) - S(0) \le -\frac{\eta}{L}t_{\mathrm{r}} \end{cases} \tag{30}$$

The time of reaching the sliding surface can be calculated as

$$t_{\mathrm{r}} \le \frac{S(0)L}{\eta} \tag{31}$$

When $S \le 0$, the time to reach the sliding surface is

$$t_{\mathrm{r}} \le -\frac{S(0)L}{\eta} \tag{32}$$

According to the sliding surface (22), when the system reaches the sliding surface, the observed current can be guaranteed to be equal to the actual current, so the observed current value converges from any initial state to the real current value in finite time t_{r}.

If the sliding mode disturbance observer and the double closed-loop controller of buck converter are started synchronously, the initial state of the observer is $v_{\mathrm{dc}}(0)$=48V, $v_{\mathrm{B}}(0)$=48V, $v_{\mathrm{o}}(0)$=0V, $i_{\mathrm{dc}}(0)$=0A, $i_{\mathrm{L}}(0)$=0A, $\hat{i}_{\mathrm{L}}(0) = 0$. In this initial state, $S(0) = 0$ and $t_{\mathrm{r}} = 0$s. If the sliding mode observer is started after the double closed-loop operation is stable, the initial state of the observer is $v_{\mathrm{dc}}(0)$=48V, $v_{\mathrm{B}}(0)$=48V, $v_{\mathrm{o}}(0)$=24V, $i_{\mathrm{dc}}(0)$=2.4A, $i_{\mathrm{L}}(0)$=0A, $\hat{i}_{\mathrm{L}}(0) = 0$. In this initial state, $S(0) = 2.4$. When $\sigma = 800$ and $\eta = 50$, $t_{\mathrm{r}} = 2.4\text{e-}6$s.

Since the convergence time t_{r} of the sliding mode observer is much shorter than the self-excited oscillation period (1.915e-3s) of the LC filter, it can be considered that

$$\hat{v}_{\mathrm{B}}(t) = v_{\mathrm{B}}(t) \tag{33}$$

IV. INPUT ADMITTANCE SHAPING METHOD FOR BUCK CONVERTER

A. OBSERVED VOLTAGE FEEDFORWARD

In order to suppress the self-excited oscillation of the LC filter, the observed voltage is feedforward to the current loop through the filter. According to Fig.5(b), the output voltage of buck converter changes to

$$v_{\mathrm{o}}(s) = \frac{DV_{\mathrm{M}}T_{\mathrm{c}}(s)\,v_{\mathrm{B}}(s)}{V_{\mathrm{in}}C_{\mathrm{i}}(s)\,C_{\mathrm{v}}(s)} + \frac{\beta C_{\mathrm{f}}(s)\,T_{\mathrm{c}}(s)}{C_{\mathrm{v}}(s)}\hat{v}_{\mathrm{B}}(s) \tag{34}$$

The input current of buck converter becomes

$$i_{\mathrm{in}}(s) = \left(-\frac{I_{\mathrm{L}}C(s)}{V_{\mathrm{M}}} + \frac{D}{Z_{\mathrm{cr}}(s)}\right)v_{\mathrm{o}}(s) + \frac{\beta I_L C_{\mathrm{f}}(s)\,C_{\mathrm{i}}(s)}{V_{\mathrm{M}}}\hat{v}_{\mathrm{B}}(s) \tag{35}$$

The input admittance of buck converter can be obtained by simultaneous equations (25), (26) and (27) as

$$Y_{\mathrm{inc}}(s) = Y_{\mathrm{in}}(s) + Y_{\mathrm{v}}(s) \tag{36}$$

where Y_{v} is the virtual admittance as follows

$$Y_{\mathrm{v}}(s) = \frac{\beta V_{\mathrm{B}}C_{\mathrm{i}}(s)\,C_{\mathrm{f}}(s)}{DV_{\mathrm{M}}}Y_{\mathrm{in}}(s) + \frac{\beta I_L C_{\mathrm{i}}(s)\,C_{\mathrm{f}}(s)}{V_{\mathrm{M}}}$$

Fig.5(c) shows the equivalent control diagram of the system after feedforward compensation. It can be seen that the feedforward compensation constructs a feedback branch $Y_{\mathrm{v}}(s)$ in parallel with $Y_{\mathrm{in}}(s)$, which is equivalent to a parallel impedance in the buck converter. The amplitude and phase of the impedance ratio are adjusted by changing the virtual admittance $Y_{\mathrm{v}}(s)$ to suppress the LC filter's self-excited oscillation.

B. STABILITY OF AMPLITUDE SHIPING

The amplitude of the impedance ratio $Z_{\mathrm{of}}(s)Y_{\mathrm{in}}(s)$ is greater than 1, and the phase is $(2\mathrm{n}+1)\pi$ at the resonant frequency of the LC input filter, and the LC filter resonates. One effective method to suppress LC filter self-excited oscillation is to change the amplitude of impedance ratio $Z_{\mathrm{of}}(s)Y_{\mathrm{in}}(s)$.

In the feedforward compensation link $C_{\mathrm{f}}(s)$, a second-order low-pass filter with high-quality factor is selected as follows

$$C_{\mathrm{lp}}(s) = \frac{\omega_0^2}{s^2 + \frac{\omega_0}{Q}s + \omega_0^2} \tag{37}$$

where Q is the quality factor and ω_0 is the resonant frequency of the second-order low-pass filter. Because the high resonance peak of the LC input filter causes the impedance ratio's amplitude to be greater than 1, the peak gain of the LC input filter needs to be reduced. The resonance frequency ω_0 of

the second-order low-pass filter is chosen as the resonance frequency $2\pi f_r$ of the LC input filter.

Although a low-pass filter introduces the DC component of the input voltage, the DC component's effect can be offset by the integral link of the voltage outer loop. The high resonance peak of the high-quality factor second-order low-pass filter is used to compensate for the input admittance of the buck converter. Fig.6(a) is a Bode diagram of the buck converter's input admittance after feedforward compensation. The feedforward coefficient β is 0.05 and the quality factor Q is 7.5. At the resonance frequency (522Hz), the admittance amplitude changes to -41dB ($|Y_{inc}(s)| = 0.009$), and the phase also changes slightly. The second-order low-pass filter changes the admittance amplitude and phase near the resonance frequency but does not affect other bands' admittance. Fig.6(b) is a Bode diagram of the impedance ratio $Z_{of}(s)Y_{inc}(s)$ after feedforward compensation. At the resonance frequency, the phase of the impedance ratio $Z_{of}(s)Y_{inc}(s)$ is still equal to π, but the amplitude of the impedance ratio $Z_{of}(s)Y_{inc}(s)$ changes to -4.66dB, ($|Z_{of}(s)Y_{inc}(s)| = 0.59$). Fig.6(c) is a Nyquist diagram of $Z_{of}(s)Y_{inc}(s)$. It can be seen from the diagram that the Nyquist curve of the system no longer contains $(-1,0)$ point and the stability margin is significantly improved after compensation. The magnitude of impedance ratio $Z_{of}(s)Y_{inc}(s)$ is less than 1 in the whole frequency domain after the compensation of the second-order low-pass filter. The amplitude shipping method can guarantee that the LC filter does not satisfy the starting conditions of self-excited oscillation and suppresses the LC filter's self-excited oscillation.

C. STABILITY OF PHASE SHIPING

Based on the starting and balance conditions of the self-excited oscillation, the system oscillation can also be suppressed by guaranteeing that the impedance ratio phase is not equal to $(2n+1)\pi$ where the amplitude of the impedance ratio is greater than or equal to 1.

Selecting Band-pass Filter in Feedback Compensation Link $C_f(s)$

$$C_{bp1}(s) = \frac{s}{s+\omega_h}\frac{\omega_l}{s+\omega_l} \tag{38}$$

or

$$C_{bp2}(s) = \frac{s}{s+\omega_h}\frac{\omega_l}{s+\omega_l}\frac{\omega_l}{s+\omega_l} \tag{39}$$

where ω_h is the cutoff frequency of the high-pass filter and ω_l is the cutoff frequency of the low-pass filter. The frequency band whose impedance ratio amplitude is greater than or equal to 1 needs to be compensated, so $\omega_h < 2\pi f_r < \omega_l$.

Fig.7(a) is a Bode diagram of the input admittance and Fig.7(b) is a Bode diagram of the impedance ratio $Z_{of}(s)Y_{inc}(s)$ after feedforward compensation by a band-pass filter with a feedforward coefficient of $\beta = 2, \omega_h = 820$rad/s, and $\omega_l = 3240$rad/s. When $C_f(s) = C_{bp1}(s)$, the maximum admittance value changes to -16.7dB ($|Y_{inc}(s)| = 0.15$), and the phase at the resonance frequency (522Hz)

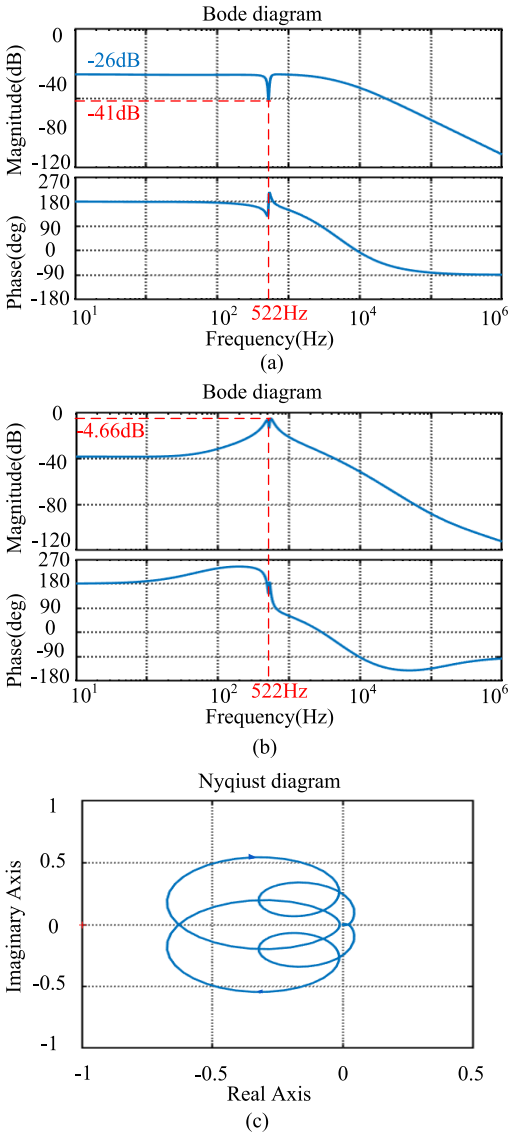

FIGURE 6. Characteristic curve of buck converter after low pass filter compensation: (a) Input admittance Bode diagram of buck converter, (b) Bode diagram of $Z_{of}(s)Y_{inc}(s)$, (c) Nyquist diagram of $Z_{of}(s)Y_{inc}(s)$.

changes to 45.2deg. Fig.7(b) shows that the impedance ratio $Z_{of}(s)Y_{inc}(s)$ changes to 9.76dB ($|Z_{of}(s)Y_{inc}(s)| = 3.08$) at the resonance frequency (522Hz), but the phase of impedance ratio is between 0-180deg and not equal to 180deg when the impedance ratio is greater than 1. It ensures that the LC filter does not satisfy the starting conditions of the self-excited oscillation, thus suppressing the self-excited oscillation of the LC filter.

When $C_f(s) = C_{bp2}(s)$, the admittance phase changes to 343 deg at the resonance frequency (522Hz), as shown in Fig.7(a). Fig.7(b) shows that the impedance ratio $Z_{of}(s)Y_{inc}(s)$ changes to 3.03dB ($|Z_{of}(s)Y_{inc}(s)| = 1.42$) at the resonance frequency (522Hz), and the phase between 180 deg and 540deg when the impedance ratio is greater than 1. After the compensation of the band-pass filter, the phase is not equal to $(2n+1)\pi$ when the amplitude of the impedance ratio

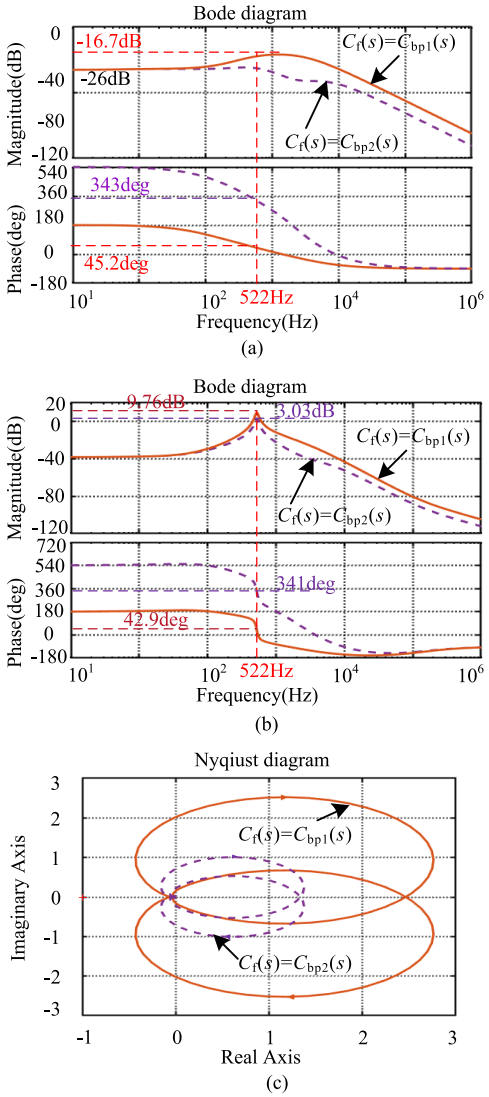

FIGURE 7. Characteristic curve of buck converter after Band-pass filter compensation: (a) Input admittance Bode diagram of buck converter, (b) Bode diagram of $Z_{of}(s)Y_{inc}(s)$, (c) Nyquist diagram of $Z_{of}(s)Y_{inc}(s)$.

$Z_{of}(s)Y_{inc}(s)$ is greater than 1, and the amplitude is less than 1 when the phase is equal to $(2n+1)\pi$. The band-pass filter ensures that the system does not meet the two conditions of self-excited oscillation simultaneously and then suppresses the self-excited oscillation of the LC filter.

V. EXPERIMENT TESTS

To verify the validity of the proposed method, a hardware device is built, as shown in Fig.8, including LC filter, buck circuit, load, drive circuit, sensor and control circuit. The circuit parameters of the LC filter and buck converter are shown in Table 1.

A. HARMONIC SUPPRESSION AND SELF-OSCILLATION OF LC FILTER

The current harmonic suppression of the LC filter is verified, and the current waveform is shown in Fig. 9 (a). The input

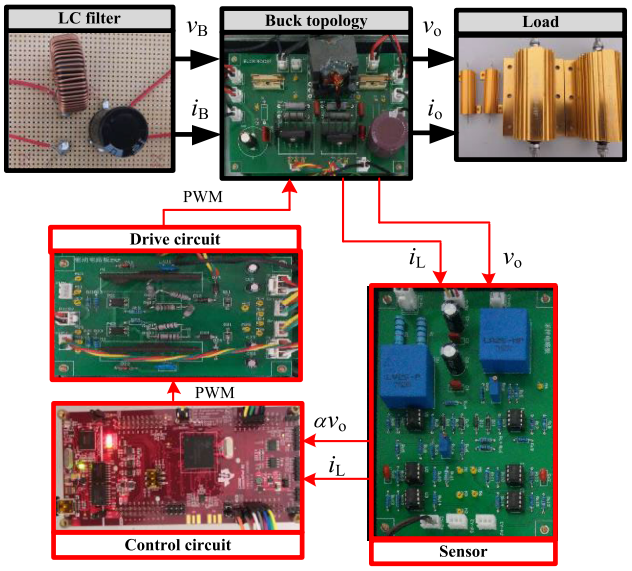

FIGURE 8. Schematic diagram of the experimental device.

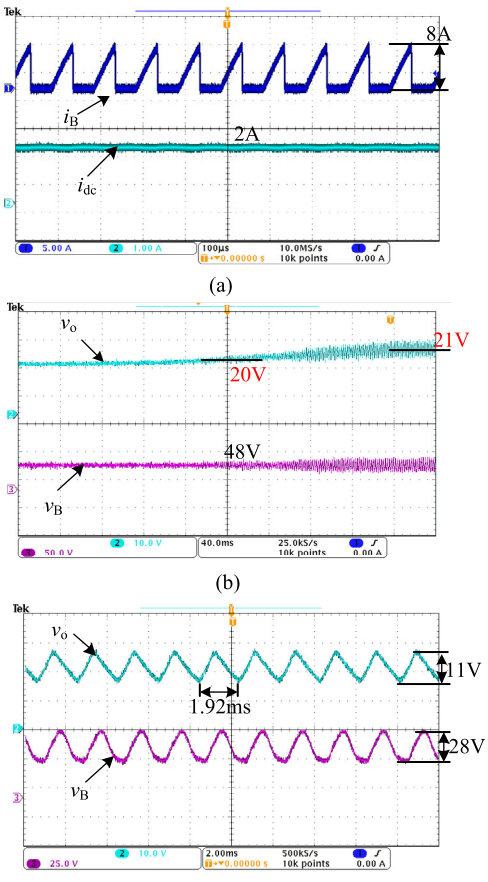

FIGURE 9. The filtering effect of LC filter and the phenomenon of self-oscillation: (a) Input current of LC filter and the buck converter, (b) Self-excited oscillation of LC filter, (c) Local figure of oscillation voltage.

current of the buck converter is intermittent sawtooth with a maximum peak of 8A. The input current of the LC filter is a stable DC current with a value of 2A. It can be seen that

the LC filter can suppress the current harmonics of the buck converter.

The stability of the system without feedforward compensation is also tested. Fig.9(b), (c) are the unstable voltage waveform of the buck converter and the oscillating waveform's local amplification respectively. The input voltage of the LC filter is stable at 48V. Theoretical analysis shows that the LC filter produces self-excited oscillation when the buck converter's power is 115W. To observe the self-oscillation phenomenon, the buck converter's load resistance is chosen to be 5Ω, and the reference voltage of the buck converter is slowly raised. The input and output voltage of the buck converter starts to oscillate when the output voltage of the buck converter increases to 20V. When the output voltage of the buck converter reaches 21V, the power of the buck converter is 88W, the oscillation amplitude of the output voltage is 5.5V, the oscillation amplitude of the input voltage is 14V, and the oscillation period is 1.92 ms (the oscillation frequency is 521 Hz). If the reference voltage is continuously increased, the oscillation amplitude would increase, which could lead to system protection, so the output voltage only rised to 21V. The resonance frequency is not consistent with the theoretical value (522 Hz). There are two main reasons: 1) there is some error in inductance and capacitance parameters; 2) 522 Hz is the starting frequency at which $|Z_{of}(s)Y_{in}(s)| = 1.26$, rather than the oscillation frequency when the amplitude is stable. The experimental results are consistent with the theoretical analysis and verify the correctness of the cascade system's resonance mechanism.

B. EXPERIMENT OF INPUT ADMITTANCE SHAPING

This experiment verified the suppression of $C_{lp}(s)$, $C_{bp1}(s)$ and $C_{bp2}(s)$ on the self-excited oscillation of the LC filter. Fig.10(a) is the experimental waveform using $C_{lp}(s)$ for the feedforward loop. When the power of buck converter changes from 57W to 115W, the input voltage of buck converter decreases by 0.4V, the maximum oscillation amplitude of dynamic process is 3V, and the dynamic attenuation process lasts 40ms. The buck converter's output voltage always maintains 24V, the maximum oscillation amplitude of the dynamic process is 1.5V, and the dynamic adjustment time is 64ms.

Fig.10(b) is an experimental waveform using $C_{bp1}(s)$ for the feedforward loop. When the power of buck converter changes from 57W to 115W, the buck converter's input voltage is reduced by 0.4V, the maximum oscillation amplitude of dynamic process is still 3V, but the dynamic attenuation process is shortened to 25ms. The stable value of the output voltage is always 24V, the maximum oscillation amplitude of the dynamic process is 1V, and the dynamic adjustment time is 34ms. Fig.10(c) is an experimental waveform using $C_{bp2}(s)$ for the feedforward loop. When the buck converter's power changes from 57W to 115W, the input voltage of the buck converter decreases by 0.4V, the maximum oscillation amplitude of the dynamic process is 2V, and the dynamic attenuation process is also 25ms. The steady-state value of the buck converter's output voltage is always maintained at 24V,

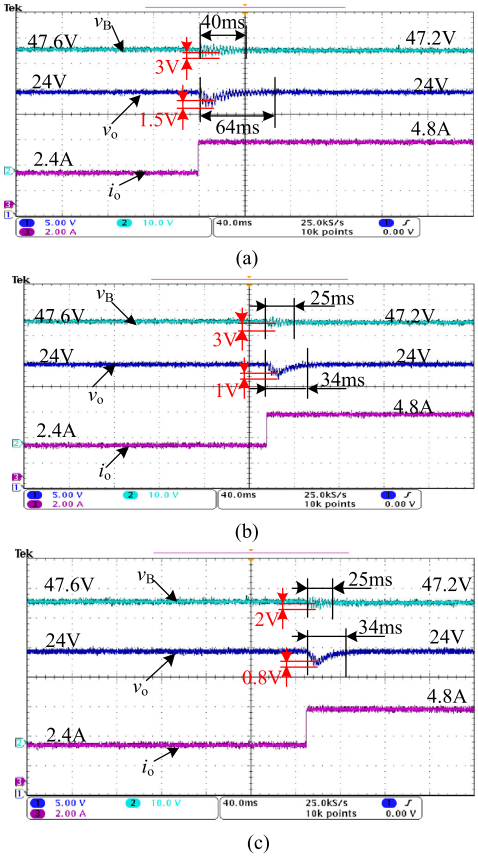

FIGURE 10. Feedforward compensation experiment: (a) Feedforward compensator is the low-pass filter $C_{lp}(s)$, (b) Feedforward compensator is the band-pass filter $C_{bp1}(s)$, (c) Feedforward compensator is the band-pass filter $C_{bp2}(s)$.

the maximum oscillation amplitude of the dynamic process is 0.8V, and the dynamic adjustment time is also 34ms.

VI. CONCLUSION

In order to solve the problem of self-excited oscillation of the LC input filter caused by buck converter, a phase shaping method for negative input admittance of buck converter is proposed. The theoretical derivation and experimental results are as follows

(1) When the impedance ratio $Z_{of}(s)Y_{in}(s)$ satisfies the starting conditions, it would cause self-excited oscillation of the LC filter.

(2) The impedance phase shaping method based on observed voltage feedforward can effectively solve the problem of the LC filter's self-excited oscillation.

(3) The sliding mode disturbance observer reduces the number of voltage sensors and reduces the hardware cost.

(4) The dynamic characteristics of the impedance phase shaping method are better than that of the impedance amplitude shaping method.

REFERENCES

[1] U. Javaid, F. D. Freijedo, D. Dujic, and W. van der Merwe, "Dynamic assessment of Source–Load interactions in marine MVDC distribution," *IEEE Trans. Ind. Electron.*, vol. 64, no. 6, pp. 4372–4381, Jun. 2017, doi: 10.1109/TIE.2017.2674597.

[2] Zhang, Zhuang, Liu, Wang, and Guo, "A novel autonomous current-sharing control strategy for multiple paralleled DC–DC converters in islanded DC microgrid," *Energies*, vol. 12, no. 20, p. 3951, Oct. 2019, doi: 10.3390/en12203951.
[3] Q. Zhang, X. Zhuang, Y. Liu, C. Wang, and H. Guo, "A novel control strategy for mode seamless switching of PV converter in DC microgrid based on double integral sliding mode control," *ISA Trans.*, vol. 100, pp. 469–480, May 2020, doi: 10.1016/j.isatra.2019.12.013.
[4] P. Magne, B. Nahid-Mobarakeh, and S. Pierfederici, "Dynamic consideration of DC microgrids with constant power loads and active damping System—A design method for fault-tolerant stabilizing system," *IEEE J. Emerg. Sel. Topics Power Electron.*, vol. 2, no. 3, pp. 562–570, Sep. 2014, doi: 10.1109/jestpe.2014.2305979.
[5] M. Wu and D. D.-C. Lu, "A novel stabilization method of LC input filter with constant power loads without load performance compromise in DC microgrids," *IEEE Trans. Ind. Electron.*, vol. 62, no. 7, pp. 4552–4562, Jul. 2015, doi: 10.1109/TIE.2014.2367005.
[6] S. Du, B. Wu, and N. R. Zargari, "A startup method for flying-capacitor modular multilevel converter (FC-MMC) with effective damping of LC oscillations," *IEEE Trans. Power Electron.*, vol. 32, no. 7, pp. 5827–5834, Jul. 2017, doi: 10.1109/TPEL.2016.2613513.
[7] M. S. Sadabadi and Q. Shafiee, "Scalable robust voltage control of DC microgrids with uncertain constant power loads," *IEEE Trans. Power Syst.*, vol. 35, no. 1, pp. 508–515, Jan. 2020, doi: 10.1109/TPWRS.2019.2928512.
[8] M. E. Fouda, A. Allagui, A. S. Elwakil, A. Eltawil, and F. Kurdahi, "Supercapacitor discharge under constant resistance, constant current and constant power loads," *J. Power Sources*, vol. 435, Sep. 2019, Art. no. 226829, doi: 10.1016/j.jpowsour.2019.226829.
[9] S.-W. Lee and J. Kim, "Small-signal modeling, integration, and hardware implementation for optimized DC distribution system based on hierarchical control master–slave structure," *Electric Power Syst. Res.*, vol. 177, Dec. 2019, Art. no. 105998, doi: 10.1016/j.epsr.2019.105998.
[10] Q. Xu, C. Zhang, C. Wen, and P. Wang, "A novel composite nonlinear controller for stabilization of constant power load in DC microgrid," *IEEE Trans. Smart Grid*, vol. 10, no. 1, pp. 752–761, Jan. 2019, doi: 10.1109/TSG.2017.2751755.
[11] N. Rashidirad, M. Hamzeh, K. Sheshyekani, and E. Afjei, "High-frequency oscillations and their leading causes in DC microgrids," *IEEE Trans. Energy Convers.*, vol. 32, no. 4, pp. 1479–1491, Dec. 2017, doi: 10.1109/TEC.2017.2698476.
[12] F. Paz and M. Ordonez, "High-accuracy impedance detection to improve transient stability in microgrids," *IEEE Trans. Ind. Electron.*, vol. 64, no. 10, pp. 8167–8176, Oct. 2017, doi: 10.1109/TIE.2017.2694405.
[13] M. A. Bianchi, I. G. Zurbriggen, F. Paz, and M. Ordonez, "Improving DC microgrid dynamic performance using a fast State-Plane-Based source-end controller," *IEEE Trans. Power Electron.*, vol. 34, no. 8, pp. 8062–8078, Aug. 2019, doi: 10.1109/TPEL.2018.2878383.
[14] S. Yousefizadeh, J. D. Bendtsen, N. Vafamand, M. H. Khooban, F. Blaabjerg, and T. Dragicevic, "Tracking control for a DC microgrid feeding uncertain loads in more electric aircraft: Adaptive backstepping approach," *IEEE Trans. Ind. Electron.*, vol. 66, no. 7, pp. 5644–5652, Jul. 2019, doi: 10.1109/TIE.2018.2880666.
[15] Y. Feng, X. Nie, and X. Chen, "Robust optimal filtering over lossy networks," *IEEE Trans. Autom. Control*, vol. 65, no. 5, pp. 2272–2277, May 2020, doi: 10.1109/TAC.2019.2942555.
[16] F. Li, X. Li, X. Zhang, and C. Yang, "Asynchronous filtering for delayed Markovian jump systems via homogeneous polynomial approach," *IEEE Trans. Autom. Control*, vol. 65, no. 5, pp. 2163–2170, May 2020, doi: 10.1109/TAC.2019.2938843.
[17] J. Wu and Y. Lu, "Adaptive backstepping sliding mode control for boost converter with constant power load," *IEEE Access*, vol. 7, pp. 50797–50807, 2019, doi: 10.1109/ACCESS.2019.2910936.
[18] Z. Cheng, M. Gong, J. Gao, Z. Li, and J. Si, "Research on virtual inductive control strategy for direct current microgrid with constant power loads," *Appl. Sci.*, vol. 9, no. 20, p. 4449, Oct. 2019, doi: 10.3390/app9204449.
[19] S. Liu, P. Su, and L. Zhang, "A virtual negative inductor stabilizing strategy for DC microgrid with constant power loads," *IEEE Access*, vol. 6, pp. 59728–59741, 2018, doi: 10.1109/ACCESS.2018.2874201.
[20] S. Liu, P. Su, and L. Zhang, "A nonlinear disturbance observer based virtual negative inductor stabilizing strategy for DC microgrid with constant power loads," *Energies*, vol. 11, no. 11, p. 3174, Nov. 2018, doi: 10.3390/en11113174.
[21] M. N. Hussain, R. Mishra, and V. Agarwal, "A frequency-dependent virtual impedance for voltage-regulating converters feeding constant power loads in a DC microgrid," *IEEE Trans. Ind. Appl.*, vol. 54, no. 6, pp. 5630–5639, Nov. 2018, doi: 10.1109/TIA.2018.2846637.
[22] S. Yousefizadeh, J. D. Bendtsen, N. Vafamand, M. H. Khooban, T. Dragicevic, and F. Blaabjerg, "EKF-based predictive stabilization of shipboard DC microgrids with uncertain time-varying load," *IEEE J. Emerg. Sel. Topics Power Electron.*, vol. 7, no. 2, pp. 901–909, Jun. 2019, doi: 10.1109/JESTPE.2018.2889971.
[23] H. Wang, X. Ge, and Y.-C. Liu, "An active damping stabilization scheme for the suppression of the DC-link oscillation in metro traction drive system," *IEEE Trans. Ind. Appl.*, vol. 54, no. 5, pp. 5113–5123, Sep. 2018, doi: 10.1109/TIA.2018.2849719.
[24] Y. A.-R.-I. Mohamed, A. A. A. Radwan, and T. K. Lee, "Decoupled Reference-Voltage-Based active DC-link stabilization for PMSM drives with tight-speed regulation," *IEEE Trans. Ind. Electron.*, vol. 59, no. 12, pp. 4523–4536, Dec. 2012, doi: 10.1109/TIE.2011.2182013.
[25] M. Wu, D. D.-C. Lu, and C. K. Tse, "Direct and optimal linear active methods for stabilization of LC input filters and DC/DC converters under voltage mode control," *IEEE J. Emerg. Sel. Topics Circuits Syst.*, vol. 5, no. 3, pp. 402–412, Sep. 2015, doi: 10.1109/JETCAS.2015.2462171.
[26] J. Liu, L. Wu, C. Wu, W. Luo, and L. G. Franquelo, "Event-triggering dissipative control of switched stochastic systems via sliding mode," *Automatica*, vol. 103, pp. 261–273, May 2019, doi: 10.1016/j.automatica.2019.01.029.
[27] F. Li, C. Du, C. Yang, L. Wu, and W. Gui, "Finite-time asynchronous sliding mode control for Markovian jump systems," *Automatica*, vol. 109, Nov. 2019, Art. no. 108503, doi: 10.1016/j.automatica.2019.108503.

XUZHOU ZHUANG (Graduate Student Member, IEEE) was born in Shandong, China, in 1989. He received the B.S. and M.S. degrees in marine engineering from Dalian Maritime University, Dalian, China, in 2013 and 2018, respectively, where he is currently pursuing the Ph.D. degree in marine engineering. His current research interests include power electronics, stability control of the nonlinear system in ship dc micro-grid, and non-linear sliding mode control.

QINJIN ZHANG (Member, IEEE) born in Jiangsu, China, in 1986. He received the B.S. degree in electrical engineering and automation, and the M.S. and Ph.D. degrees in marine engineering from Dalian Maritime University, Dalian, China, in 2009, 2011, and 2015, respectively. Since 2016, he has been a Lecturer with the Marine Engineering College, Dalian Maritime University. His current research interests include distributed energy generation technology, power electronics converters, microgrids, and ship dc integrated power systems.

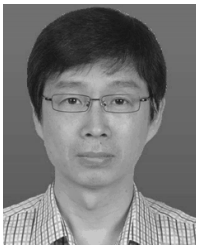

YANCHENG LIU was born in Liaoning, China. He received the B.S. and M.S. degrees in electrical engineering from Harbin Industrial University, Harbin, China, in 1985 and 1988, respectively, and the Ph.D. degree in marine engineering from Dalian Maritime University, Dalian, China, in 2002. He is currently a Professor with the Marine Engineering College, Dalian Maritime University. His current research interests include ac motor control, power electronic converters, ship electrical propulsion technology, renewable energy systems, and microgrids.

PENGLI ZHU (Graduate Student Member, IEEE) received the B.Eng. degree in marine engineering and the M.Eng. degree in naval architecture and ocean engineering from Dalian Maritime University (DMU), Dalian, China, in 2017 and 2020, respectively, where he is currently pursuing the Ph.D. degree. His current research interests include perception analysis and intelligent control of unmanned underwater vehicles.

XIANGLU ZHENG was born in Shandong, China. He received the B.S. degrees in ship electronic and electrical engineering from Dalian Maritime University, Dalian, China, in 2018, where he is currently pursuing the M.D. degree in ship and ocean engineering. His current research interests include active damping stability control of the source-load system in ship dc micro-grid and parallel stability control of dc-dc power converters.

YUJI ZENG was born in Guangdong, China, in 1996. He received the B.S. degrees in marine engineering from Guangdong Ocean University, Zhanjiang, China, in 2018. He is currently pursuing the M.D. degree in marine engineering with Dalian Maritime University, Dalian, China. His current research interests include ship dc microgrid energy storage system control and dc microgrid coordinated operation control.

HAOHAO GUO was born in Jiangxi, China, in 1984. He received the M.S. and B.S. degrees from the Marine Engineering College, Dalian Maritime University, Dalian, China, in 2007 and 2012, respectively. He is currently a Lecturer with the Marine Engineering College, Dalian Maritime University. Since 2019, he has been a Visiting Scholar with Aalborg University, Denmark. His current research interests include ship electrical propulsion technology and PMSM control.

ZHENRUI ZHANG (Graduate Student Member, IEEE) was born in Shandong, China, in 1994. He received the B.S. degree in marine engineering from Yantai University, Yantai, China, in 2017. He is currently pursuing the Ph.D. degree in marine engineering with Dalian Maritime University, Dalian, China. His research interest includes sensor-less control technology for PMSM.